

Three-dimensional ResNet for efficient prediction of ground state phases in multicomponent dipolar spinor BECs

Chengji Liao(廖承继), Tiantian Li(李甜甜), Xiao-Dong Bai(柏小东), and Yunbo Zhang(张云波)
Citation: Chin. Phys. B, 2025, 34 (**7**): 076701. DOI: 10.1088/1674-1056/adc7f9
http://cpb.iphy.ac.cn; http://iopscience.iop.org/cpb

What follows is a list of articles you may be interested in

Coherence of nonlinear Bloch dynamics of Bose—Einstein condensates in deep optical lattices

Ai-Xia Zhang(张爱霞), Wei Zhang(张薇), Jie Wang(王杰), Xiao-Wen Hu(胡潇文), Lai-Lai Mi(米来来), and Ju-Kui Xue(薛具奎)
Chin. Phys. B, 2024, 33 (**4**): 040305. DOI: 10.1088/1674-1056/ad1b46

Special breathing structures induced by bright solitons collision in a binary dipolar Bose-Einstein condensates

Gen Zhang(张根), Li-Zheng Lv(吕李政), Peng Gao(高鹏), and Zhan-Ying Yang(杨战营)
Chin. Phys. B, 2023, 32 (**11**): 110303. DOI: 10.1088/1674-1056/acf283

Nonlinear modes coupling of trapped spin-orbit coupled spin-1 Bose-Einstein condensates

Jie Wang(王杰), Jun-Cheng Liang(梁俊成), Zi-Fa Yu(鱼自发), An-Qing Zhang(张安庆),Ai-Xia Zhang(张爱霞), and Ju-Kui Xue(薛具奎)
Chin. Phys. B, 2023, 32 (**9**): 090305. DOI: 10.1088/1674-1056/accd53

Cluster mean-field study of spinor Bose-Hubbard ladder: Ground-state phase diagram and many-body population dynamics

Li Zhang(张莉), Wenjie Liu(柳文洁), Jiahao Huang(黄嘉豪), and Chaohong Lee(李朝红)
Chin. Phys. B, 2021, 30 (**2**): 026701. DOI: 10.1088/1674-1056/abd760

Phase diagram and collective modes in Rashba spin–orbit coupled BEC: Effect of in-plane magnetic field

Dong Dong (董冬), Zou Xu-Bo (邹旭波), Guo Guang-Can (郭光灿)
Chin. Phys. B, 2015, 24 (**7**): 076701. DOI: 10.1088/1674-1056/24/7/076701

Three-dimensional ResNet for efficient prediction of ground state phases in multicomponent dipolar spinor BECs

Chengji Liao(廖承继)[1], Tiantian Li(李甜甜)[1,†], Xiao-Dong Bai(柏小东)[2], and Yunbo Zhang(张云波)[3]

[1] *School of Physics and Optoelectronics, Xiangtan University, Xiangtan* 411100, *China*
[2] *College of Physics and Hebei Key Laboratory of Photophysics Research and Application, Hebei Normal University, Shijiazhuang* 050024, *China*
[3] *Department of Physics, Zhejiang Sci-Tech University, Hangzhou* 310018, *China*

(Received 24 February 2025; revised manuscript received 28 March 2025; accepted manuscript online 2 April 2025)

Machine learning has rapidly become a powerful tool for addressing challenges in ultracold atomic systems; however, its application to intricate three-dimensional (3D) systems remains relatively underexplored. In this study, we introduce a 3D residual network (3D ResNet) framework based on 3D convolutional neural networks (3D CNN) to predict ground states phases in 3D dipolar spinor Bose–Einstein condensates (BECs). Our results show that the 3D ResNet framework predicts ground states with high accuracy and efficiency across a broad parameter space. To enhance phase transition predictions, we incorporate data augmentation techniques, leading to a notable improvement in the model's performance. The method is further validated in more complex scenarios, particularly when transverse magnetic fields are introduced. Compared to conventional imaginary-time evolution methods (ITEM), the 3D ResNet drastically reduces computational costs, offering a rapid and scalable solution for complex 3D multi-parameter nonlinear systems.

Keywords: 3D ResNet, ground state phases prediction, data augmentation

PACS: 67.85.Fg, 03.75.Mn, 05.30.Rt, 07.05.Mh

DOI: 10.1088/1674-1056/adc7f9 **CSTR:** 32038.14.CPB.adc7f9

1. Introduction

The dipole–dipole interaction in spinor BEC, characterized by its long-range nature and anisotropic properties, plays a crucial role in shaping the condensate's physical characteristics, giving rise to novel quantum phases and excitation modes.[1–10] Furthermore, it induces a range of spin structures and dynamic behaviors, including quantum vortex lattices,[11–14] spin vortices,[15] and quantum droplets.[16–18] Recently, an experimentally realized dipolar molecule BEC, composed of sodium–caesium molecules, has demonstrated extended lifetimes.[19] Moreover, the interplay between dipolar and spin-exchange interactions has been shown to induce a variety of quantum phases.[20] For instance, under strong dipolar interactions, it can spontaneously form spin-vortex states.[21,22]

At present, the ground state of spinor BEC is typically solved using the imaginary-time evolution method (ITEM).[23] However, the convergence precision becomes more challenging with the inclusion of nonlocal dipole–dipole interactions, especially in the case of a 3-component dipolar spinor BEC in a 3D system. Furthermore, the precision of convergence is sensitive to both the initial conditions and algorithmic settings.[24] This significantly increases both computational time and resource consumption. Consequently, there is a pressing need for the development of faster and more efficient methods to solve the ground state.

In recent years, machine learning (ML) has advanced rapidly in fields such as artificial intelligence,[25] visual processing,[26–28] and scientific computing.[29–32] As a powerful data analysis tool, ML has demonstrated considerable potential in the study of ultracold atomic and quantum many-body systems. For example, ML has been successfully employed to enhance imaging data processing,[33] classify phase diagrams,[34] and solve ground states as well as investigate dynamics in many-body systems.[35–37] Mainstream neural networks, such as deep neural networks (DNNs),[38] physics-informed neural networks (PINNs),[39] and theory-guided neural networks (TgNNs),[40] have been effectively applied to various physical systems.[41–45] However, most applications have focused on one- or two-dimensional (2D) systems, leaving the optimization of 3D, multi-component systems with large datasets as a significant challenge.

Drawing inspiration from 3D CNN[46,47] and residual networks (ResNet),[48] we propose a 3D residual network framework (3D ResNet) to investigate ground state phases in 3D dipolar spinor BEC systems. In this study, the optimized 3D ResNet efficiently computes ground states across the entire parameter space without the need for iterative refinement. Moreover, the 3D ResNet more accurately identifies phase transition boundaries, even in the presence of an external magnetic field, outperforming traditional neural networks.

The remainder of this paper is structured as follows. In

†Corresponding author. E-mail: ttli@xtu.edu.cn

© 2025 Chinese Physical Society and IOP Publishing Ltd. All rights, including for text and data mining, AI training, and similar technologies, are reserved.

Section 2, we introduce the model of the 3D dipolar spinor BEC. In Section 3, we present the network structure and optimization details. In Section 4, we demonstrate that 3D ResNet can accurately predict ground states, and its performance is further enhanced by data augmentation. Finally, we conclude in Section 5.

2. Model

We consider the condensate of N spin $F=1$ atoms trapped in a double potential well, which is formed by applying a Gaussian barrier to the harmonic potential

$$U(\boldsymbol{r})=\frac{1}{2}M(\omega_\perp^2x^2+\omega_\perp^2y^2+\omega_z^2z^2)+A\,\mathrm{e}^{-z^2/(2\sigma_0^2)}, \quad (1)$$

where M is the atomic mass, $\omega_\perp$ is the radial trap frequency, ω_z is the axial trap frequency, and A and σ_0 are the height and width of the Gaussian barrier, respectively.[22] In the mean-field treatment, the condensate wavefunction $\psi_\alpha(\boldsymbol{r})$ $(\alpha=0,\pm1)$ satisfies the coupled dynamical equations[49–51]

$$\mathrm{i}\hbar\frac{\partial\psi_\alpha}{\partial t}=(T+U+c_0n)\psi_\alpha+g_\mathrm{F}\mu_\mathrm{B}\boldsymbol{B}_\mathrm{eff}\cdot\boldsymbol{F}_{\alpha\beta}\psi_\beta, \quad (2)$$

where $T=-\hbar^2\nabla^2/(2M)$ is the kinetic energy, $c_0=4\pi\hbar^2(a_0+2a_2)/(3M)$ is the spin-independent strength of the collisional interaction, a_f $(f=0,2)$ is the s-wave scattering length of two atoms with spin-1 in a combinatorially symmetric channel with total spin f, $n(\boldsymbol{r})=\sum_\alpha|\psi_\alpha|^2$ is the total particle number density, g_F is the Landé g-factor of the atom, μ_B is the Bohr magneton, and $\boldsymbol{F}$ is the angular momentum operator. The effective magnetic field $\boldsymbol{B}_\mathrm{eff}$ consists of three components, the external magnetic field $\boldsymbol{B}_\mathrm{ext}$, the spin-exchange collision interaction $\boldsymbol{B}_\mathrm{col}$, and the dipolar interaction $\boldsymbol{B}_\mathrm{dip}$,

$$\boldsymbol{B}_\mathrm{eff}(\boldsymbol{r})=\boldsymbol{B}_\mathrm{ext}+\boldsymbol{B}_\mathrm{col}(\boldsymbol{r})+\boldsymbol{B}_\mathrm{dip}(\boldsymbol{r}), \quad (3)$$

$$\boldsymbol{B}_\mathrm{col}(\boldsymbol{r})=\frac{c_2}{g_\mathrm{F}\mu_\mathrm{B}}\boldsymbol{S}(\boldsymbol{r}), \quad (4)$$

$$\boldsymbol{B}_\mathrm{dip}(\boldsymbol{r})=\frac{c_\mathrm{d}}{g_\mathrm{F}\mu_\mathrm{B}}\int\frac{\mathrm{d}\boldsymbol{r}'}{|\boldsymbol{R}|^3}\left[\boldsymbol{S}(r')-\frac{3\left[S(\boldsymbol{r}'\cdot\boldsymbol{R})\right]\boldsymbol{R}}{|\boldsymbol{R}|^2}\right], \quad (5)$$

where $c_2=4\pi\hbar^2(a_2-a_0)/(3M)$, $\boldsymbol{S}(\boldsymbol{r})=\sum_{\alpha\beta}\psi_\alpha^*\boldsymbol{F}_{\alpha\beta}\psi_\beta$ is the spin density, $\boldsymbol{R}=\boldsymbol{r}-\boldsymbol{r}'$, $c_\mathrm{d}=\mu_0\mu_\mathrm{B}^2g_\mathrm{F}^2/(4\pi)$, and μ_0 is the vacuum permeability.

We compute the ground state for various values of A using the ITEM.[22] However, ITEM requires a large number of iterations to converge, particularly for 3D systems. Even with careful parameter tuning, the iterative process remains computationally intensive and time-consuming. To address these limitations, we propose the adoption of a 3D ResNet to efficiently and rapidly predict ground states.

3. Methodology

Since its introduction for behavior recognition tasks, 3D CNN have shown remarkable performance in various fields, including medical imaging, hyperspectral image processing, and video analysis.[52–54] The advantages of 3D CNN in feature extraction and high-dimensional data processing have become even more pronounced with the continuous optimization of their architectures.[55,56] However, as network depth increases, optimizing the model becomes progressively more challenging, particularly when applied to complex physical systems. To improve training efficiency and network performance, we introduce ResNet which effectively address issues such as gradient vanishing in deep architectures.[57]

In a multicomponent dipolar spinor BEC system, solving the ground state is considerably more complex compared to the single-component case. For instance, the system described by Eq. (2) requires extremely high precision (10^{-14}) for convergence, and it usually takes more than a week to compute a ground state using ITEM. Moreover, the ground state encompasses over 5×10^6 data points in 3D space, leading to a computationally intensive process when calculating the ground state across the entire parameter space. To efficiently extract high-dimensional features, we have designed a 3D ResNet architecture, incorporating 3D CNN and residual structures. Additionally, to enhance the network's generalization capabilities in complex physical systems, we incorporate data augmentation techniques.

The architecture of the three-dimensional (3D) ResNet is illustrated in Fig. 1. The input data are represented as (A,σ_0,x,y,z), where x, y, z are the spatial coordinates, and A and σ_0 correspond to the depth and width of the Gaussian barrier, respectively. Initially, the input data are passed through a convolutional layer (Conv), followed by batch normalization (BN) and an ReLU activation function for feature extraction. The data then sequentially pass through four residual blocks, with the number of layers in each block being 3, 4, 6, and 3, respectively. Each residual block consists of a convolutional layer, a batch normalization layer, an ReLU activation function, and a shortcut connection, as illustrated in the inset of Fig. 1. The shortcut connections are defined as $y=F(x)+x$, where the input is directly added to the output, thereby preserving the original information in deeper layers and alleviating the vanishing gradient issue. Finally, the data undergoes adaptive average pooling, followed by a fully connected layer. The output is the ground state wave function, consisting of three components, represented as a multidimensional array.

To optimize the training process, the 3D ResNet employs the mean squared error (MSE) as the loss function, which quantifies the discrepancy between the predicted and true values:

$$L=\frac{1}{N_\mathrm{D}}\sum_{i=1}^{N_\mathrm{D}}(\Psi_i-\Psi_i^\mathrm{NN})^2, \quad (6)$$

where N_D is the total number of training data points, and Ψ_i and Ψ_i^NN represent the true value and predicted value of the

neural network, respectively. To minimize the loss function, we employ the Adam optimization algorithm and L_2 regularization to mitigate overfitting. To alleviate the computational burden, we downscale the data by half using interpolation. The error is controlled to approximately 10^{-8} both before and after processing, ensuring feasibility. The entire network architecture is implemented in PyTorch and trained with GPU acceleration, significantly improving computational efficiency. Additionally, to improve the generalization ability of the network, we incorporate data augmentation techniques such as random rotation and Gaussian noise addition.[58] The process of adding Gaussian noise starts with calculating the standard deviation of the input data, which is then multiplied by a fixed percentage (1%) to determine the standard deviation of the noise. Using PyTorch functions, Gaussian noise with a mean of 0 and a standard deviation equal to the computed noise standard deviation is generated, ensuring it matches the shape of the input data. The generated noise is then added to the input data, while the labels remain unchanged, resulting in an augmented dataset of the same size as the original training set. For random rotation, a PyTorch function is employed to randomly select an angle between 0 and 2π, and the data are rotated around two spatial axes. Both the inputs and labels are transformed simultaneously, producing a new dataset. The introduction of Gaussian noise is equivalent to applying a slight perturbation to the input parameters. This not only increases sample diversity but also mimics the Tikhonov regularization mechanism,[59] encouraging the network to learn global features. Random rotation enhances the spatial representation of the data, enabling the model to achieve more stable and accurate predictions, especially in the sensitive region of phase transition critical points.[58]

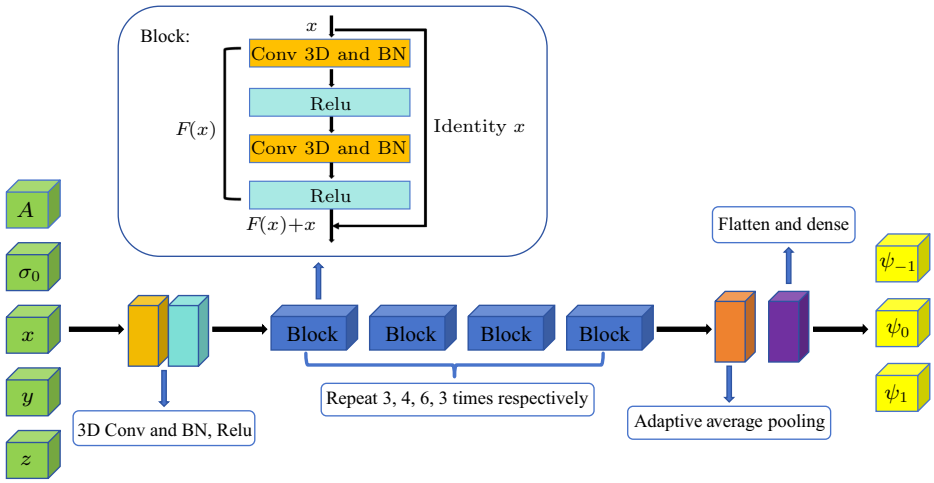


Fig. 1. The structure of 3D ResNet.

4. Results

To evaluate the prediction accuracy of the network, we quantitatively evaluate the results by R^2 score and L_2 error, defined as

$$R^2 = 1 - \frac{\sum_{i=1}^{N}(\Psi_i^{\mathrm{NN}} - \Psi_i)^2}{\sum_{i=1}^{N}(\bar{\Psi} - \Psi_i)^2}, \tag{7}$$

$$L_2 = \frac{\left\|\Psi^{\mathrm{NN}} - \Psi\right\|_2}{\|\Psi\|_2}, \tag{8}$$

where $\|\cdot\|_2$ is the standard Euclidean norm, N is the number of evaluation points, $\bar{\Psi}$ is the average of the true values, and Ψ^{NN} and Ψ represent the predicted and real values of the 3D ResNet for a set of parameters, respectively. The R^2 score measures the predictive capacity of the network, where values closer to 1 indicate superior performance. The L_2 error quantifies the difference between the predicted and real values, where values closer to 0 indicate better.

4.1. Prediction ability of the ground state

To evaluate the prediction ability of the 3D ResNet, we predict the ground state of the system described by Eq. (2). The effective magnetic field for this system is given in Eq. (3), with the external magnetic field set to $\boldsymbol{B}_{\mathrm{ext}} = 0$. The training set consists of 12 data points, with the width σ_0 fixed and the height A sampled at 25 intervals from 0 to 300. The ground states for these parameters are solved using ITEM. The number of training rounds is set to 8000, and the initial learning rate is set to 5×10^{-4}, which is halved after every 1000 rounds. We evaluate the prediction accuracy using R^2 and L_2, as shown in Table 1.

First, we select test points close to the training points, such as $A = 60, 160, 260$. We find that the 3D ResNet achieves high prediction accuracy: the R^2 scores are close to 1 (0.99) and the L_2 errors are close to 0 (10^{-8}). Then, we select test points slightly further from the training points, such as $A = 10, 237, 320$. Although the prediction accuracy decreases slightly, as indicated by $R^2 = 0.97$ and $L_2 = 2 \times 10^{-7}$, it still

provides good prediction results. However, when we select test points near the phase transition point (red values in Table 1), we observe a significant decrease in accuracy: R^2 drops to 0.2 and L_2 increases to 7×10^{-6}. The results indicate that the 3D ResNet performs excellently in predicting the ground state in non-phase transition regions, but its prediction ability is limited in phase transition regions. In fact, determining phase transition points is also challenging in numerical simulations, especially in the context of machine learning. To address this issue, we have employed several strategies which are detailed in the following section.

Table 1. The R^2 and L_2 at different A.

A	R^2	L_2
10	9.6189×10^{-1}	3.4527×10^{-7}
60	9.9129×10^{-1}	7.8725×10^{-8}
160	9.8993×10^{-1}	9.0727×10^{-8}
237	9.7784×10^{-1}	1.9965×10^{-7}
245	2.3291×10^{-1}	6.9105×10^{-6}
246	1.8881×10^{-1}	7.3077×10^{-6}
260	9.8934×10^{-1}	9.6242×10^{-8}
320	9.7735×10^{-1}	2.0514×10^{-7}

4.2. Enhancing prediction accuracy through data augmentation in phase transition regions

To improve the prediction ability of the 3D ResNet in phase transition regions, we employ two data augmentation techniques: Gaussian noise addition and random rotation. Prediction accuracy is further assessed by analyzing the spin structure of the condensate, as described by Eq. (2). The spin structure of the ground state results from the interplay between interwell dipole–dipole interactions and the tunneling splitting of the double-well potential. When $A<246$, the condensates exhibit a parallel spin-vortex pair structure, while for $A>246$, the vortex structure transitions to an antiparallel spin-vortex pair.[22]

We select four test points near the phase transition point ($A=246$) to compare the prediction accuracy with and without data augmentation (see Table 2). We find that some of the test points are poorly predicted without data augmentation. For $A=245$ and $A=246$, without data augmentation, R^2 is only 0.2 and L_2 increases to 7×10^{-6}, indicating significant prediction errors. After applying data augmentation, R^2 increases substantially, L_2 decreases, and the prediction accuracy improves effectively. For $A=247$ and $A=248$, the 3D ResNet prediction accuracy is high without data augmentation and improves further with data augmentation.

Furthermore, we present the vortex structure predicted by the 3D ResNet after applying data augmentation, as shown in Fig. 2. It successfully predicts the transition of the spin structure from a parallel vortex pair (Figs. 2(a) and 2(c)) to an antiparallel vortex pair (Figs. 2(b) and 2(d)). The results are consistent with the traditional numerical solution, indicating that data augmentation effectively improves the prediction accuracy of the 3D ResNet in the phase transition region.

Table 1. Comparisons of R^2 and L_2 for no data augmentation versus data augmentation.

	R^2		L_2	
A	No data augmentation	Data augmentation	No data augmentation	Data augmentation
(245)	2.3291×10^{-01}	8.7061×10^{-01}	6.9105×10^{-06}	1.1656×10^{-06}
(246)	1.8881×10^{-01}	9.8358×10^{-01}	7.3077×10^{-06}	1.4873×10^{-07}
(247)	9.7136×10^{-01}	9.8833×10^{-01}	2.5945×10^{-07}	1.0568×10^{-07}
(248)	9.7855×10^{-01}	9.8948×10^{-01}	1.9433×10^{-07}	9.5247×10^{-08}

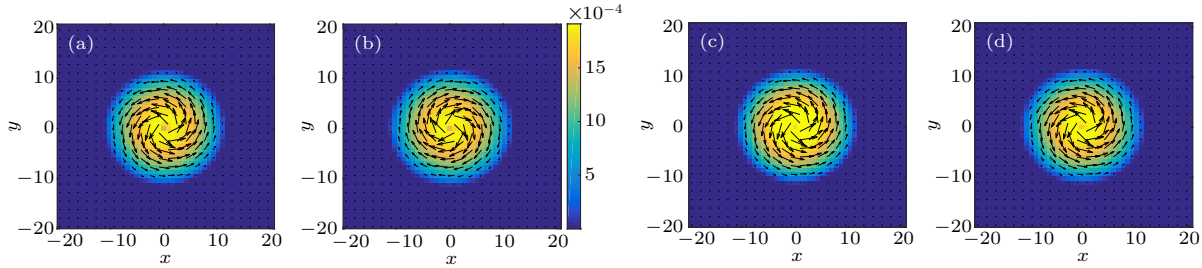


Fig. 2. Slices of the vortex structure predicted by the 3D ResNet near the phase transition point after data augmentation. Panels (a) and (c) show the vortex slices for $A=245$, $\sigma_0=0.65$ at the planes of maximum density along the the z-axis. Panels (b) and (d) show the vortex slices for $A=247$, $\sigma_0=0.65$ at the planes of maximum density along the z-axis.

4.3. Comprehensive validation of data augmentation

To further assess the improvement of the 3D ResNet's prediction ability in the phase transition region with data augmentation, we introduce the external magnetic field $\boldsymbol{B}_{\rm ext}=B_x$ in Eq. (3) to increase the complexity of the system. For a parallel vortex pair ($A=100$), as B_x increases, the system transitions through three phases, with the number of vortices decreasing from 2 to 1 (red values in Table 3), and finally to 0 (blue values in Table 3).

Compared to the previous parts, the input parameters for the 3D ResNet include an additional B_x, namely, (A,B_x,σ_0,x,y,z). To avoid unintended bias, we select points

uniformly within the parameter range as the training set and focus on selecting test points near the phase transition points. Table 3 lists the training and test sets, while Table 4 compares the prediction accuracy of the 3D ResNet with and without data augmentation. We further validated that data augmentation effectively improves the prediction accuracy in the phase transition region. Although the prediction accuracy of the 3D ResNet for non-phase transition points (black values in Table 3) is already high without data augmentation, it further improves with the application of data augmentation. For phase transition points, such as $(A = 100,\ B_x = 56)$ and $(A = 100,\ B_x = 65)$, the R^2 without data augmentation is only 0.3, and L_2 is increases to 8×10^{-6}. After applying data augmentation, R^2 increases, L_2 decreases, and accuracy improves significantly. Further analysis shows that when $A = 100$, B_x undergoes two phase transitions in the range of 50–70, which increases the prediction difficulty of the 3D ResNet.

Generally, the 3D ResNet predicts vortex structures accurately without data augmentation in most cases. However, near phase transition points, the prediction accuracy of the vortex structure decreases. For instance, for $(A = 100,\ B_x = 56)$, figures 3(a) and 3(d) show that the lower vortex structure is predicted accurately, but the upper vortex structure is less precise. After applying data augmentation, as shown in Figs. 3(b) and 3(e), the predictions become more accurate, closely matching the true values shown in Figs. 3(c) and 3(f). These results further validate that data augmentation improves prediction accuracy, especially in the phase transition region.

Table 3. Training and test sets for $A = 100$ and $A = 300$ at different transverse magnetic fields B_x.

A	Training set B_x	Test set B_x
100	0, 10, 20, 30, 40, 50, 60, 70, 80	35, 45,56,57, 65, 66
300	0, 10, 20, 30, 40, 50, 60, 70, 80	35, 42, 43, 55, 56, 65

Table 4. Comparison of R^2 and L_2 for no data augmentation vs. data augmentation.

	R^2		L_2	
A, B_x	No data augmentation	Data augmentation	No data augmentation	Data augmentation
(100, 35)	9.8255×10^{-01}	9.8427×10^{-01}	1.5528×10^{-07}	1.3997×10^{-07}
(100, 45)	9.8036×10^{-01}	9.8248×10^{-01}	1.7411×10^{-07}	1.5529×10^{-07}
(100, 56)	3.2874×10^{-01}	9.6239×10^{-01}	8.9379×10^{-06}	3.3207×10^{-07}
(100, 57)	8.7073×10^{-01}	9.6880×10^{-01}	1.1505×10^{-06}	2.7769×10^{-07}
(100, 65)	3.2737×10^{-01}	8.4529×10^{-01}	8.8634×10^{-06}	1.3743×10^{-06}
(100, 66)	9.5865×10^{-01}	9.8846×10^{-01}	3.6325×10^{-07}	1.0131×10^{-07}
(300, 35)	9.6466×10^{-01}	9.8045×10^{-01}	3.2021×10^{-07}	1.7707×10^{-07}
(300, 42)	9.5836×10^{-01}	9.7372×10^{-01}	3.7739×10^{-07}	2.3816×10^{-07}
(300, 43)	8.9791×10^{-01}	9.2016×10^{-01}	9.2539×10^{-07}	7.2359×10^{-07}
(300, 55)	9.5479×10^{-01}	9.7255×10^{-01}	4.1011×10^{-07}	2.4895×10^{-07}
(300, 56)	9.5304×10^{-01}	9.6812×10^{-01}	4.2619×10^{-07}	2.8933×10^{-07}
(300, 65)	9.6831×10^{-01}	9.8564×10^{-01}	2.8764×10^{-07}	1.3026×10^{-07}

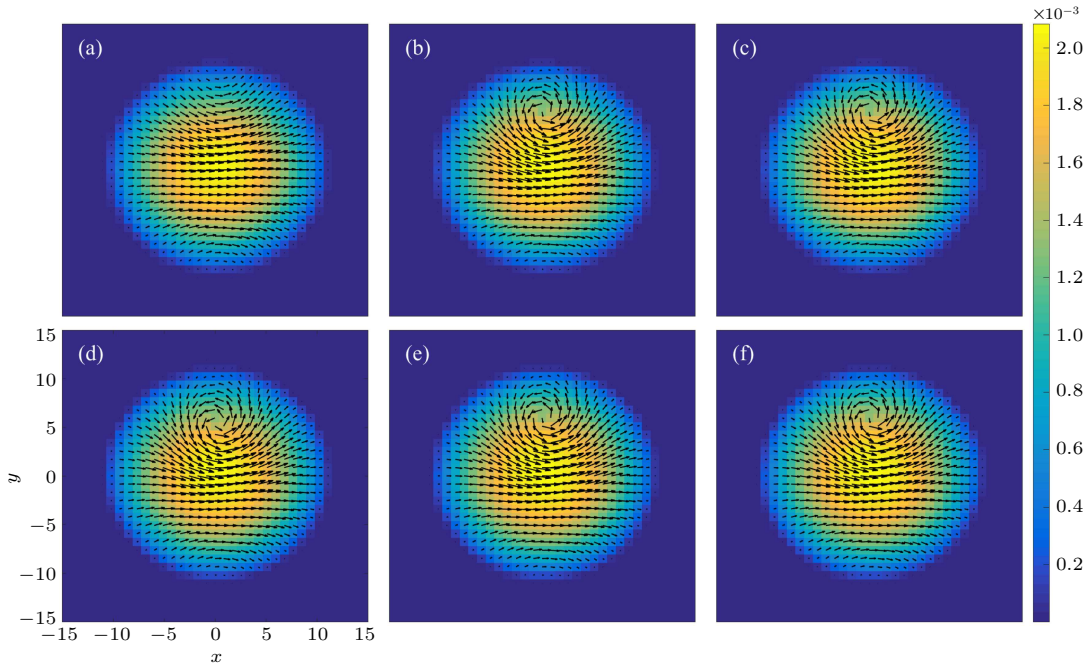


Fig. 3. Predicted vortex structure of the 3D ResNet at the phase transition point $A = 100$, $B_x = 56$. Panels (a) and (d) show predicted values without data augmentation, panels (b) and (e) show predicted values with data augmentation, panels (c) and (f) display the real values using the traditional numerical method.

In addition, we compare the computational efficiency of the 3D ResNet with traditional numerical methods. In this case, the GPU-based 3D ResNet completes 8000 epochs in approximately 50 minutes while using 20 GB of memory, with subsequent predictions taking about 0.6 s per data point. In contrast, traditional CPU-based methods, such as ITEM, require over a week per parameter set, even when parallelized on a 72-core cluster (processing four cases at 100% utilization). Moreover, solving each new parameter set necessitates repeating the full iterative process, which becomes particularly challenging in phase transition regions due to numerical convergence difficulties.

5. Conclusions

In this paper, we designed and validated a 3D ResNet for predicting ground state phases in 3D multicomponent dipolar spinor BEC systems. The 3D ResNet, using only a small amount of ITEM data, can accurately predict arbitrary ground states across the entire parameter space, bypassing the need for the computationally expensive iterative processes required by traditional methods. We also improved the model's prediction accuracy in the phase transition region through data augmentation. The enhanced model's effectiveness is further validated across systems with transverse magnetic fields.

In comparison to ITEM, the 3D ResNet offers substantial improvements in computational efficiency, enabling faster training, and predictions for complex 3D systems. This framework shows potential for extension to other 3D multicomponent systems.

Acknowledgment

Project supported by the National Natural Science Foundation of China (Grant Nos. 11904309 and 12305015), the Natural Science Foundation of Hunan Province, China (Grant No. 2020JJ5528), and the Natural Science Foundation of Hebei Province, China (Grant No. A2024205027).

References

[1] Santos L, Shlyapnikov G V, Zoller P, *et al.* 2002 *Phys. Rev. Lett.* **88** 139904
[2] Lahaye T, Menotti C, Santos L, *et al.* 2009 *Rep. Prog. Phys.* **72** 126401
[3] Tang Y, Kao W, Li K Y, *et al.* 2018 *Phys. Rev. Lett.* **120** 230401
[4] Chomaz L, Baier S, Petter D, *et al.* 2016 *Phys. Rev. X* **6** 041039
[5] Tanzi L, Roccuzzo S M, Lucioni E, *et al.* 2019 *Nat. Phys.* **574** 382
[6] Baillie D and Blakie P B 2018 *Phys. Rev. Lett.* **121** 195301
[7] Wenzel M, Böttcher F, Schmidt J N, *et al.* 2018 *Phys. Rev. Lett.* **121** 030401
[8] Zhang F and Yin L 2023 *Chin. Phys. Lett.* **40** 066701
[9] Zhang G, Lv L Z, Gao P, *et al.* 2023 *Chin. Phys. B* **32** 110303
[10] Lan Z Z 2024 *Chin. Phys. Lett.* **41** 090501
[11] Prasad S B, Bland T, Mulkerin B C, *et al.* 2019 *Phys. Rev. A* **100** 023625
[12] Kumar R K, Tomio L, Malomed B A, *et al.* 2017 *Phys. Rev. A* **96** 063624
[13] Ancilotto F and Reatto L 2024 *Phys. Rev. A* **110** 013302
[14] Jiang Y, Qi R, Shi Z Y, *et al.* 2017 *Phys. Rev. Lett.* **118** 080403
[15] Vengalattore M, Leslie S R, Guzman J, *et al.* 2008 *Phys. Rev. Lett.* **100** 170403
[16] Li G, Zhao Z, Jiang X, *et al.* 2024 *Phys. Rev. Lett.* **133** 053804
[17] Li S and Saito H 2024 *Phys. Rev. Res.* **6** L042049
[18] Yoğurt T A, Tanyeri U, Keleş A, *et al.* 2003 *Phys. Rev. A* **108** 033315
[19] Bigagli N, Yuan W, Zhang S, *et al.* 2024 *Nature* **631** 289
[20] Yi S and Pu H 2006 *Phys. Rev. Lett.* **97** 020401
[21] Kawaguchi Y, Saito H and Ueda M 2006 *Phys. Rev. Lett.* **97** 130404
[22] Li T, Yi S and Zhang Y 2015 *Phys. Rev. A* **92** 063603
[23] Chiofalo M L, Succi S and Tosi M P 2000 *Phys. Rev. E* **62** 7438
[24] Motta M, Sun C, Tan A T K, *et al.* 2020 *Nat. Phys.* **16** 205
[25] Silver D, Huang A, Maddison C, *et al.* 2016 *Nature* **529** 484
[26] Krizhevsky A, Sutskever I and Hinton G E 2017 *Commun. ACM* **60** 84
[27] Simonyan K and Zisserman A 2014 arXiv: 1409.1556
[28] Dosovitskiy A, Beyer L, Kolesnikov A, *et al.* 2020 arXiv:2010.11929
[29] Raissi M, Perdikaris P and Karniadakis G E 2019 *J. Comput. Phys.* **378** 686
[30] Bar-Sinai Y, Hoyer S, Hickey J, *et al.* 2019 *Proc. Natl. Acad. Sci. USA* **116** 15344
[31] Han J, Zhang L and Weinan E 2019 *J. Comput. Phys.* **399** 108929
[32] Brunton S L and Kutz J N 2024 *Nat. Comput. Sci.* **4** 483
[33] Vendeiro Z, Ramette J, Rudelis A, *et al.* 2022 *Phys. Rev. Res.* **4** 043216
[34] Link M, Gao K, Kell A, *et al.* 2023 *Phys. Rev. Lett.* **130** 203401
[35] Bai X D and Zhang D 2022 *Phys. Rev. E* **106** 025305
[36] Guo S, Koh S M, Fritsch A R, *et al.* 2022 *Phys. Rev. Res.* **4** 023163
[37] Bai X D and Zhang D 2021 *Phys. Rev. A* **104** 063316
[38] Miao W, Linghu Z, Du Q, *et al.* 2023 *Chin. Phys. Lett.* **40** 014301
[39] Raissi M, Perdikaris P and Karniadakis G E 2019 *J. Comput. Phys.* **378** 686
[40] Wang N, Zhang D, Chang H, *et al.* 2020 *J. Hydrol.* **584** 124700
[41] Karniadakis G E, Kevrekidis I G, Lu L, *et al.* 2021 *Nat. Rev. Phys.* **3** 422
[42] Meng Z, Qian Q, Xu M, *et al.* 2023 *Comput. Methods Appl. Mech. Eng.* **414** 116172
[43] Kuang J, Bai X D, Du W, *et al.* 2024 *Results Phys.* **64** 107935
[44] Tian S, Cao C and Li B 2023 *Results Phys.* **52** 106842
[45] Liu J, Wang W, Xia H, *et al.* 2024 *Results Phys.* **61** 107716
[46] Ji S, Xu W, Yang M, *et al.* 2013 *IEEE Trans. Pattern Anal. Mach. Intell.* **35** 221
[47] Tran D, Bourdev L, Fergus R, *et al.* 2015 *IEEE Int. Conf. Comput. Vis.* **4489–4497**
[48] He K, Zhang X, Ren S, *et al.* 2016 *IEEE Conf. Comput. Vis. Pattern Recognit.* **770–778**
[49] Ho T L 1998 *Phys. Rev. Lett.* **81** 742
[50] Ohmi T and Machida K 1998 *J. Phys. Soc. Jpn.* **67** 1822
[51] Zhang J N, He L, Pu H, *et al.* 2009 *Phys. Rev. A* **79** 033615
[52] Çiçek Ö, Abdulkadir A, Lienkamp S S, *et al.* 2016 *MICCAI* **9901**
[53] Carreira J and Zisserman A 2017 *IEEE Conf. Comput. Vis. Pattern Recognit.* **4724–4733**
[54] Li S, Song W, Fang L, *et al.* 2019 *IEEE Trans. Geosci. Remote Sens.* **57** 6690
[55] Tran D, Bourdev L, Fergus R, *et al.* 2015 *IEEE Int. Conf. Comput. Vis.* **4489–4497**
[56] Li Y, Zhang H and Shen Q 2017 *Remote Sens.* **9** 67
[57] Peida W, Cui Z, Gan Z, *et al.* 2020 *Sensors* **20** 1652
[58] Shorten C and Khoshgoftaar T M 2019 *J. Big Data* **6** 60
[59] Bishop C M 1995 *Neural Comput.* **7** 108